Monthly Notices
of the
ROYAL ASTRONOMICAL SOCIETY

MNRAS **470,** 1729–1737 (2017)
Advance Access publication 2017 June 3

doi:10.1093/mnras/stx1350

Mass evaporation rate of globular clusters in a strong tidal field

Juan P. Madrid,[1,2]★ Nathan W. C. Leigh,[3] Jarrod R. Hurley[2] and Mirek Giersz[4]

[1]*CSIRO, Astronomy and Space Science, PO BOX 76, Epping NSW 1710, Australia*
[2]*Centre for Astrophysics and Supercomputing, Swinburne University of Technology, Hawthorn, VIC 3122, Australia*
[3]*Department of Astrophysics, American Museum of Natural History, Central Park West and 79th Street, NY 10024, USA*
[4]*Nicolaus Copernicus Astronomical Centre, Polish Academy of Sciences, ul. Bartycka 18, PL-00-716 Warsaw, Poland*

Accepted 2017 May 30. Received 2017 May 30; in original form 2016 April 28

ABSTRACT

The mass evaporation rate of globular clusters evolving in a strong Galactic tidal field is derived through the analysis of large, multimass *N*-body simulations. For comparison, we also study the same evaporation rates using MOCCA Monte Carlo models for globular cluster evolution. Our results show that the mass evaporation rate is a dynamical value, that is, far from a constant single number found in earlier analytical work and commonly used in the literature. Moreover, the evaporation rate derived with these simulations is higher than values previously published. These models also show that the value of the mass evaporation rate depends on the strength of the tidal field. We give an analytical estimate of the mass evaporation rate as a function of time and galactocentric distance $\xi(R_{\rm GC}, t)$. Upon extrapolating this formula to smaller $R_{\rm GC}$ values, our results provide tentative evidence for a very high ξ value at small $R_{\rm GC}$. Our results suggest that the corresponding mass-loss in the inner Galactic potential could be high and it should be accounted for when star clusters pass within it. This has direct relevance to nuclear cluster formation/growth via the infall of globular clusters through dynamical friction. As an illustrative example, we estimate how the evaporation rate increases for an $\sim 10^5$ $M_\odot$ globular cluster that decays through dynamical friction into the Galactic Centre. We discuss the findings of this work in relation to the formation of nuclear star clusters by inspiralling globular clusters.

Key words: methods: numerical – stars: kinematics and dynamics – globular clusters: general.

1 INTRODUCTION

A more detailed examination of the evaporation rate of globular clusters (ξ) obtained through modern *N*-body models is granted given that the value of ξ is often used. A recent example is the work of Gnedin, Ostriker & Tremaine (2014) that uses the evaporation rate in their study of nuclear star cluster formation through the inspiralling of globular clusters into the galactic nuclei. The evaporation rate is also used by Gieles, Heggie & Zhao (2011) in their study of the evolution of star clusters in a tidal field.

Ambartsumian (1938) and Spitzer (1940) established a dimensionless evaporation rate ξ that takes the following expression:

$$\xi \equiv -\frac{t_{\rm rh}}{M}\frac{{\rm d}M}{{\rm d}t} \quad (1)$$

where $t_{\rm rh}$ is the half-mass relaxation time given by

$$t_{\rm rh} = \frac{0.14N}{\ln\Lambda}\sqrt{\frac{r_{\rm hm}^3}{GM}}, \quad (2)$$

where $\Lambda = 0.4N$ is the argument of the Coulomb logarithm, N is the number of stars, M the globular cluster mass, G the gravitational constant and $r_{\rm hm}$ the half-mass radius (Spitzer & Hart 1971). We should note that for single mass models, M is proportional to N.

Initial estimates of ξ were obtained analytically by Ambartsumian (1938), who found $\xi = 0.0074$ and later by Hénon (1961), who found $\xi = 0.045$. Spitzer & Chevalier (1973) recalculate the value of ξ and find that this quantity is dependent on the ratio between the tidal radius and the half-mass radius $r_t/r_{\rm hm}$. Spitzer & Chevalier (1973) find $\xi = 0.015$ and ξ=0.05 for different $r_t/r_{\rm hm}$ ratios.

Lee & Goodman (1995) carried out a detailed study of the evaporation rate for post-collapse globular clusters using a multimass Fokker–Planck code. They find that the mass-loss rate ξ is roughly constant for most of the evolution of the globular cluster – their fig. 1.

While the publications cited above are among those that established the foundations of star cluster dynamics, their results were none the less obtained making several approximations. Among the simplifications used are star clusters in isolation, that is, free from tidal interactions, star clusters with single-mass stars, just schematic stellar evolution and star clusters in the steady post core-collapse regime.

★ E-mail: jmadrid@astro.swin.edu.au

The reality underlying cluster evaporation and mass-loss, however, is much more complicated than these pioneering works cited above fully addressed. For example, the inclusion of realistic stellar evolution and the associated mass-loss breaks the one-to-one connection between mass-loss and evaporation, since stars can reduce their masses due to stellar evolution without actually evaporating from the cluster.

We have now the ability to accurately simulate globular clusters throughout an entire Hubble time of evolution. Baumgardt & Makino (2003) performed a series of *N*-body models of globular clusters in tidal fields using NBODY4. These models were used to show that stellar evolution plays an important role in the mass-loss rate of globular clusters, particularly during the early stages of their lifetimes. Baumgardt & Makino (2003) also showed how the external tidal field plays a crucial role in determining the dissolution time for globular clusters. Other studies have addressed different environmental effects on cluster disruption and mass-loss such as bulge and disc shocking (Gnedin & Ostriker 1997) and radial anisotropy (Leigh et al. 2013; Webb, Sills & Harris 2013; Brockamp et al. 2014; Webb et al. 2014).

Hong et al. (2013) make a distinction between the evaporation rate of single and multimass models of globular clusters, i.e. $\xi(N) \neq \xi(M)$. Hong et al. (2013) use a definition of the *mass evaporation rate* $\xi(M)$ that we adopt here. The mass evaporation rate that we refer through this paper is not limited to evaporation of stars from two body interactions. Our dimensionless mass evaporation rate includes all mechanisms of mass-loss. Our method folds into a single ξ parameter all physical processes of mass-loss such as tidal interactions with the host galaxy, stellar evolution, relaxation-driven mass-loss, etc.

Gieles & Baumgardt (2008) studied the escape rate of stars from tidally limited star clusters with different radii. The main differences between this work and the work of Gieles & Baumgardt (2008) are that our simulations include stellar evolution, primordial binaries and a more advanced description of the tidal field. Gieles & Baumgardt (2008) assumed a point mass potential. Also, for multimass models, star-loss rates and mass-loss rates are not equivalent, we show this in the following sections.

Here, we study the dimensionless mass-loss rates using a more sophisticated treatment for the Galactic potential than adopted in previous studies, with an emphasis on the inner regions of the Galaxy. In our simulations, the galactic potential is modelled with three distinct components: bulge, disc and halo. The additive gravitational force of each of these three components is computed for each star of the simulation.

In this work, we derive the value of ξ for globular clusters in a strong tidal field using mainly *N*-body simulations, but we also use the Monte Carlo code MOCCA, which provides results with minimal computational expense, as well as a detailed stellar evolution prescription.

Throughout this work, we consider a Hubble time to be 13.8 Gyr, in agreement with the latest cosmological findings of the Planck Collaboration XIII (2016).

2 A SIMULATED GLOBULAR CLUSTER EVOLVING IN A STRONG TIDAL FIELD

In this section, we describe the codes used to simulate globular cluster evolution. We begin with the *N*-body simulations before moving on to describe the Monte Carlo models, since our focus in this paper is the former. The Monte Carlo models are meant to complement and compare the results of our *N*-body simulations.

Table 1. Parameters of simulated star clusters.

Label	R_{GC}	N	M_i	Code
1	4 kpc	200k	1.3×10^5 M$_\odot$	NBODY6
2	4 kpc	200k	1.3×10^5 M$_\odot$	NBODY6
3	4 kpc	100k	6.3×10^4 M$_\odot$	NBODY6
4	6 kpc	100k	6.3×10^4 M$_\odot$	NBODY6
5	8 kpc	100k	6.3×10^4 M$_\odot$	NBODY6
6	10 kpc	100k	6.3×10^4 M$_\odot$	NBODY6
7	20 kpc	100k	6.3×10^4 M$_\odot$	NBODY6
8	50 kpc	100k	6.3×10^4 M$_\odot$	NBODY6
9	4 kpc	200k	1.3×10^5 M$_\odot$	MOCCA
10	50 kpc	100k	6.3×10^4 M$_\odot$	MOCCA

2.1 *N*-body simulations

2.1.1 *Models setup*

An up-to-date version of the code NBODY6 is used to carry out the simulations (Aarseth 1999). This version includes the gravitational potential of a Milky Way–type galaxy (Aarseth 2003). The Galactic potential is modelled using a bulge mass of $M_B = 1.5 \times 10^{10}$ M$_\odot$ and disc mass of $M_D = 5 \times 10^{10}$ M$_\odot$. The geometry of the disc is modelled following the formulae of Miyamoto & Nagai (1975) with the following scale parameters $a = 4.0$ kpc and $b = 0.5$ kpc. A logarithmic halo is included such that the circular velocity is 200 km s^{-1} at 8.0 kpc from the Galactic Centre. The tidal field generated by the host galaxy is taken into account for the calculation of the equations of motion of all stars within the simulated globular cluster. Our simulations begin when all the stars in the globular cluster are formed, all residual gas removed and the cluster is in a stable orbit around its host galaxy. The initial velocity distribution of stars follows virial equilibrium.

The simulations were run on Graphic Processing Units (GPUs), specifically NVIDIA Tesla C2070 cards mounted on the GPU Supercomputer for Theoretical Astrophysics Research at Swinburne University (gSTAR). The setup of these models has previously been described in detail in Madrid, Hurley & Sippel (2012) and Madrid, Hurley & Martig (2014).

We define a escape radius for stars as it was previously defined in Madrid et al. (2012, 2014). That is, stars are lost from the simulation when they have positive energy and when their distance to the centre of the cluster exceeds two tidal radii. The tidal radius (von Hoerner 1957) is a dynamical quantity, which is in turn we define using the approximation of Küpper et al. (2010):

$$r_{\rm t} \simeq \left(\frac{GM_{\rm C}}{2\Omega^2}\right)^{1/3}. \quad (3)$$

where Ω is the angular velocity.

2.1.2 *Initial conditions*

In this section, we describe a series of *N*-body models with a large number of star particles, i.e. $N = 200\,000$ (labels 1 and 2, Table 1). 5 per cent of these stars are in binary systems, that is, a total of 10 000 stars are binaries. These simulations are among the largest direct *N*-body simulations carried out to the present day (Heggie 2011, 2014; Wang et al. 2016). Each model takes about 2 months to be completed

running on one GPU. Simulations with even larger numbers of particles and initial masses would need much more computing time, since this time-scale is proportional to $N^{\sim 2-3}$, where N is the number of particles.

These simulations are multimass N-body models that follow the prescriptions of the Kroupa (2001) initial mass function (IMF). This IMF and $N = 200\,000$ yields an initial mass of $M = 1.3 \times 10^5\,\mathrm{M}_\odot$. The minimum stellar mass is $M_{\rm min} = 0.1\,\mathrm{M}_\odot$ and the maximum stellar mass is $M_{\rm min} = 50\,\mathrm{M}_\odot$. NBODY6 includes stellar and binary evolution (Hurley, Pols & Tout 2000; Hurley, Tout & Pols 2002).

The initial spatial distribution of the globular cluster follows a Plummer (1911) model and the initial metallicity is $Z = 0.001$. We should note that the Plummer model is an idealized spatial distribution altered during the first evolutionary steps by the host galaxy tidal field and internal dynamical evolution. The simulated globular cluster analysed in this section was set to evolve at a galactocentric distance of $R_{\rm gc} = 4$ kpc. At this distance from the Galactic Centre, the simulated globular cluster experiences a strong tidal field that is the additive gravitational potential of bulge and disc (Madrid et al. 2014).

The initial half-mass radius is $r_{\rm hm} = 6.2$ pc, a slightly extended cluster, and the initial tidal radius according to the standard formula is ∼52 pc, with the cluster tidally filling at birth. Stars are allowed to have orbits that go beyond the tidal radius and then return to the star cluster. As mentioned before, stars are only removed from the simulation when their orbits exceed more than two tidal radii.

As formulated in Madrid et al. (2014), our simulated star clusters have an initial inclination of ∼22.°5 with respect of the disc. With this inclination, star clusters are simulated in a general orbit as opposed to a specific co-planar or perpendicular inclination with respect of the disc. The initial inclination we use also implies that the star cluster has a maximum height of 2 kpc that is similar to the disc scale-height.

In the interest of reducing numerical uncertainties, simulations were carried out twice (labels 1 and 2, Table 1) with a different seed number for the random number generator used in the distributions that describe the initial masses, positions and velocities of the stars. Results of the otherwise identical simulations are then averaged.

2.2 Monte Carlo simulations

2.2.1 Models setup

An up-to-date version of the MOCCA code is used to carry out the Monte Carlo simulations for globular cluster evolution (Giersz et al. 2013; Hypki et al. 2013). The gravitational potential of the Milky Way is modelled with a much simpler point-mass, with a total mass equal to that of the enclosed Galaxy mass at the cluster's Galactocentric distance $R_{\rm GC}$ from the Galactic Centre. We should note that at equal host galaxy mass and equal galactocentric distance, the tidal field is stronger in a point mass potential than with a logarithmic potential. All orbits through the Galactic potential are circular within the MOCCA framework.

The simulations were performed on a PSK2 cluster at the Nicolaus Copernicus Astronomical Centre in Poland. Each simulation is run on one CPU. The cluster is based on AMD (Advanced Micro Devices, Inc.) Opteron processors with 64-bit architecture (2–2.4 GHz). The setup of these models has previously been described in detail in Giersz et al. (2013) and Leigh et al. (2013).

The MOCCA code treats the escape process in tidally limited clusters in a realistic manner as it is described in Fukushige & Heggie (2000). Here, the escape of an object from the system is not instantaneous but delayed in time. As was pointed out in Fukushige & Heggie (2000) and Baumgardt (2001), the process of escape from a cluster in a steady tidal field is complex. Some stars that fulfill the energy criterion for escape (i.e. the condition that the energy of the star exceeds the critical energy) can still be trapped inside the potential well. Some of those stars can be scattered back to lower energies before they escape from the system. These two factors cause the cluster lifetime to scale non-linearly with relaxation time for tidally limited clusters Baumgardt (2001), in contrast to what would be expected from the standard theory, see details in Giersz et al. (2013). The MOCCA simulation results are presented in Fig. 5. To minimize the statistical fluctuations connected with generation of the MOCCA initial models (labels 9 and 10, Table 1), we used exactly the same masses, positions and velocities as for the N-body runs (labels 1 and 2, Table 1).

3 MASS EVAPORATION RATE

Previous studies cited above consider the evaporation rate as a constant value during the entire lifetime of a globular cluster. As pointed out by Takahashi & Portegies Zwart (2000), the value of the evaporation rate in the calculations of Lee & Goodman (1995) is always less than 1 ($\xi < 1$) due to the absence of stellar evolution. In the models of Lee & Goodman (1995), the evaporation rate increases with time from ∼0.002 at the beginning of the globular cluster lifetime to ∼0.05. After the cluster has evolved for ∼30 per cent of its lifetime, the evaporation rate derived by Lee & Goodman (1995) asymptotes to a constant value of ∼0.05 until the cluster fully dissolves. The results of the N-body and MOCCA models performed for this study show that the behaviour of the mass evaporation rate for a cluster under a substantial tidal field varies over time and cannot be approximated by a constant single value, as shown in the top panel of Fig. 1. As mentioned above in the introduction, our dimensionless mass evaporation rate folds into a single parameter all mechanisms of mass-loss.

When stellar evolution is included in the mass evaporation rate, as we do here, ξ reaches its highest values at the beginning of the globular cluster lifetime and then decreases, which is the opposite of the results presented by Lee & Goodman (1995).

The initial value of the mass evaporation rate for the models represented in Fig. 1 is $\xi = 6.9$. The mass-loss induced by stellar evolution rapidly tapers off within the first Gyr of the star cluster lifetime and the evaporation rate decreases to $\xi < 1$ before 500 Myr.

The mass evaporation rate reaches its lowest value of $\xi = 0.07$ after a Hubble time of evolution, see Fig. 1 top panel. Even at its lowest value, ξ is higher than some previous analytical estimates (Hénon 1961; Lee & Goodman 1995). The much higher value of ξ is due to the realistic modelling of the tidal field and the inclusion of stellar evolution in the simulations.

The mass evaporation rate plotted in Fig. 1 reflects the different dominant regimes of mass-loss a globular cluster undergoes: mass-loss due to stellar evolution and mass-loss owing to tidal interactions and internal dynamics (Lamers, Baumgardt & Gieles 2010; Kruijssen et al. 2012; Leigh et al. 2012a).

Lamers et al. (2010) find three different phases of mass-loss for star clusters: (a) mass-loss dominated by stellar evolution, (b) mass-loss dominated by 'dissolution' or dynamical effects and (c) the third phase being after core collapse. Our models are in good agreement with the results of Lamers et al. (2010). In particular, we find good agreement on the rapid and early mass-loss due to stellar evolution. We also agree on the second phase of mass-loss being dominated by tidal interactions and dynamical processes.

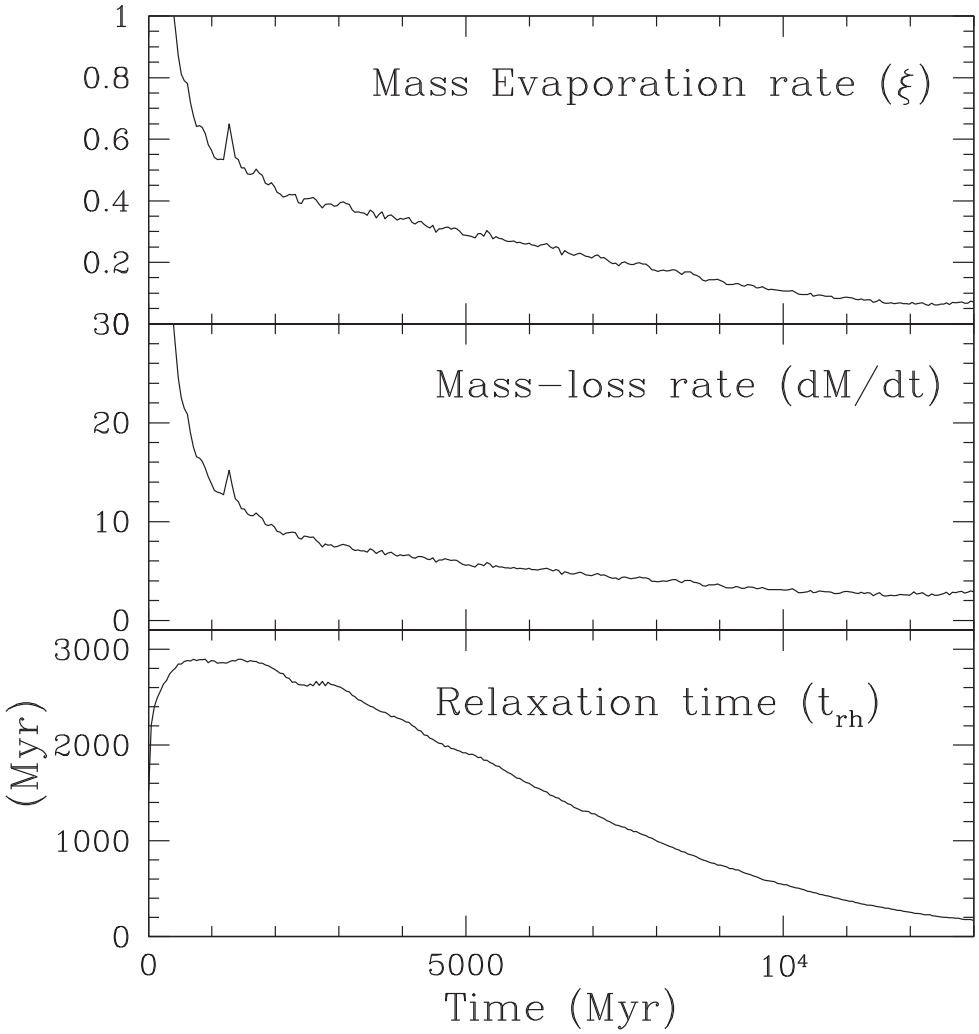

Figure 1. Mass evaporation rate (top panel) and the two physical values used in equation (1): mass-loss rate (middle panel) and half-mass relaxation time (bottom panel). The mass evaporation rate ξ of a globular cluster in a strong tidal field varies over time: an initial rapid decrease due to stellar evolution is followed by a linear decay phase. This figure uses the average values from models 1 and 2 (Table 1).

This second phase is fitted with a power law by Lamers et al. (2010) similar to what we describe and fit as a linear decay. A difference with the work of Lamers et al. (2010) is that the simulated globular clusters discussed in this section do not reach core collapse during a Hubble time of evolution. Core collapse is actually reached at 15 Gyr.

The mass evaporation rate and the first time derivative of the total globular cluster mass ($\mathrm{d}M/\mathrm{d}t$) have a bump at $\sim$1.3 Gyr. This bump is due to stellar evolution processes. At 1.3 Gyr is when the main-sequence turn-off mass is $\sim$1.8 $\mathrm{M}_{\odot}$ for a metallicity of $Z = 0.001$ (Pols et al. 1998). This is significant because it is the mass at which stars switch from having non-degenerate to degenerate cores on the giant branch. Thus, post-giant branch time-scales change and the stellar mass-loss rate changes. Also, for any binary interactions that strip giant envelopes, the resulting star will now be a helium white dwarf instead of going through a naked helium star phase, which also affects the amount of mass-loss (Hurley et al. 2000, 2002).

The evolution of the half-mass relaxation time closely follows that of the half-mass radius. For example, the early increase in $t_{\rm rh}$ is the result of an initial expansion phase for the cluster. Stellar evolution is the main driver of mass-loss during the early lifetime of globular clusters. Rapid mass-loss causes, in turn, a reduced gravitational pull resulting in an expansion. For tidally filling clusters, after the initial expansion, the half-mass radius steadily decreases as the tidal radius of the cluster decreases and in turn we see $t_{\rm rh}$ decreasing. A detailed study of the size scale of star clusters is given in Madrid et al. (2012).

NBODY6 properly accounts for the important effects of disc shocking when the star cluster is formed and settled in a stable orbit (Madrid et al. 2014). However, the early effects of impulsive shocks in the gas-rich progenitor galaxy (Kruijssen 2015) or the interactions of the star cluster with giant molecular clouds are not modelled in the current version of NBODY6. More sophisticated hydrodynamic simulations are needed to properly parametrize this correction to the dimensionless mass-loss rate.

What is the dependence of the mass evaporation rate on the initial mass of the star cluster? We can briefly address this question by comparing the two models with different initial masses (1.3×10^5 $\mathrm{M}_{\odot}$ and 6.3×10^4 $\mathrm{M}_{\odot}$ – labels 1 and 3 (Table 1). For a star cluster under the influence of a strong tidal field, i.e. on an orbit with $R_{\rm GC} = 4$ kpc, the mass evaporation rate is almost identical during the early phases of evolution when ξ is

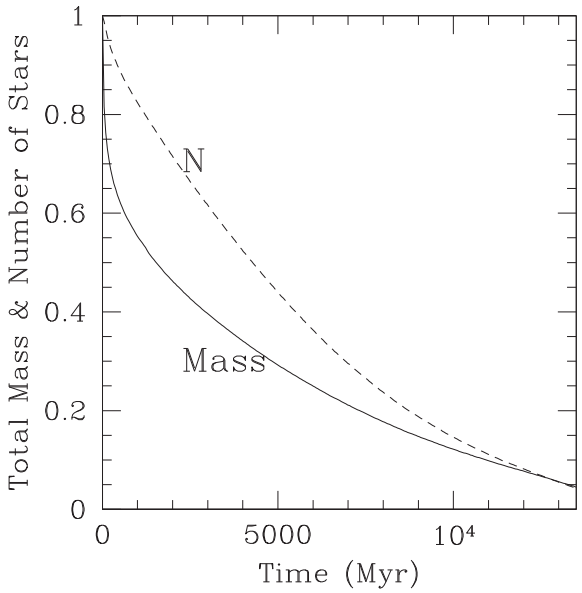

Figure 2. Total mass and number of stars remaining in the simulated star cluster. These quantities have been normalized by their initial values. This figure represents the average values for models 1 and 2 in Table 1.

dominated by mass-loss due to stellar evolution. The overall evolution of ξ is equivalent for the two models with different masses that we consider.

3.1 Total mass and number of stars

The total mass and number of stars that remain bound to the globular cluster are plotted in Fig. 3. Mass-loss rates of large *N*-body simulations have been discussed elsewhere (Madrid et al. 2012). The inclusion of stellar evolution makes the globular cluster lose mass at a faster rate than the rate at which stars are lost during the initial 12 Gyr of evolution. The mass-loss rate and star-loss rate osculate at 12 Gyr and are almost identical until dissolution.

The behaviour of the mass and number of stars over time is fundamentally different from that obtained with early work with very low *N*. In the star clusters simulated by Giersz & Heggie (1996), mass-loss and star-loss rates are identical during the initial phases of evolution to later continuously diverge until dissolution. This difference can be explained, at least in part, by a different IMF and the fact that the maximum stellar mass is higher in our simulations.

Also, the evolution of the total number of stars (N) over time, plotted in Fig. 2, is curved and different from the linear relation, followed by N in the models of Gieles et al. (2011). Our results suggest higher star-loss rates than those of the models presented by Gieles et al. (2011).

As mentioned in previous sections, earlier analytical work mostly used single mass models where $\xi(M) \equiv \xi(N)$ (Gieles et al. 2011). In Fig. 3, we plot the value of ξ as a function of mass (M) and as a function of number of stars that remain bound to the cluster (N). The latter is obtained replacing M by N on equation (1). The difference between the two expressions is naturally more pronounced during earlier stages of evolution (<3 Gyr), when $\xi(N)$ is less than $\xi(M)$. The main factor contributing to this difference is stellar evolution and the fact that we ran multimass models. Fig. 3 shows that at about 4 Gyr of tidal striping takes over stellar evolution as the main mass-loss mechanism.

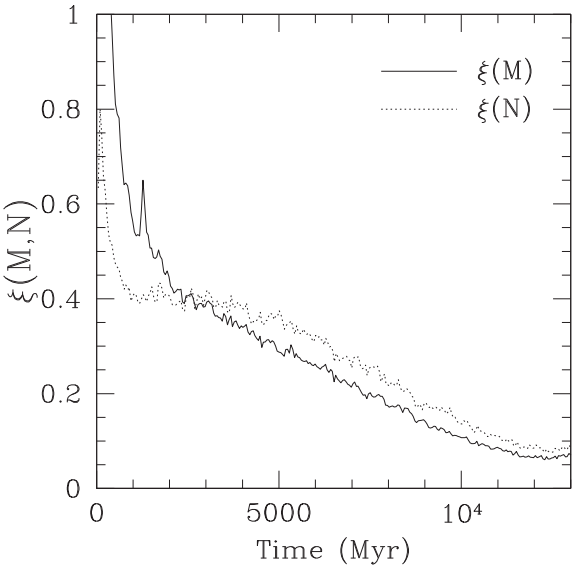

Figure 3. Dimensionless evaporation rate as function of mass $\xi(M)$ and as a function of number of stars $\xi(N)$. $\xi(N)$ is obtained by simply replacing M by N in equation (1). The difference between the two curves reflects the fact that these are multimass models that include a prescription for stellar evolution. These are the average values for models 1 and 2 in Table 1.

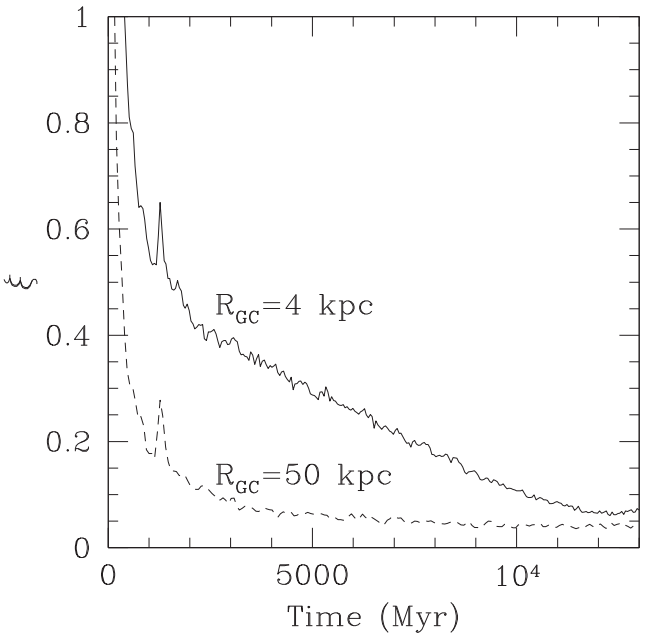

Figure 4. Time evolution of the dimensionless mass evaporation rate in our *N*-body models for a globular cluster in pseudo-isolation ($R_{GC} = 50$ kpc, dashed) and a globular cluster in a strong tidal field ($R_{GC} = 4$ kpc, solid). From the average values of models 1 and 2 (at $R_{GC} = 4$ kpc) and model 8 (at $R_{GC} = 50$ kpc).

4 RECOVERING EARLIER ANALYTICAL FINDINGS

In this section, we compare the results for a globular cluster evolving in a strong tidal field and a globular cluster in pseudo-isolation. We also show that the *N*-body and MOCCA models presented here can recover earlier analytical findings discussed in Section 1.

Fig. 4 shows the time evolution of ξ for two globular clusters in different tidal environments, taken from the results of our *N*-body

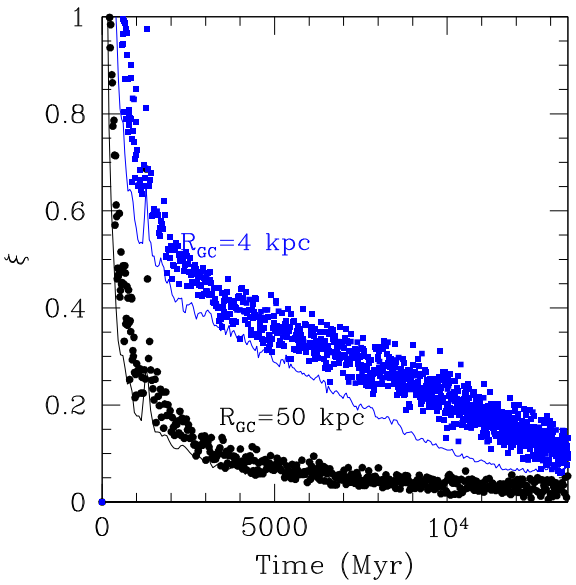

Figure 5. Time evolution of the dimensionless mass evaporation rate in our MOCCA Monte Carlo models for a globular cluster in pseudo-isolation (R_{GC} = 50 kpc, black dots) and a globular cluster in a strong tidal field (R_{GC} = 4 kpc, blue squares). The results of the *N*-body models shown in Fig. 4 are also plotted here as solid lines.

simulations. We plot in this figure the evaporation rates for globular clusters on circular orbits at 4 kpc (same as Fig. 1) and 50 kpc from the Galactic Centre. The dimensionless mass-loss rate is clearly different and thus a function of the tidal field.

The mass evaporation rate of the globular cluster evolving in pseudo-isolation at 50 kpc (label 8, Table 1) from the Galactic Centre asymptotes to a nearly constant value after ∼4 Gyr of evolution. This behaviour is in good agreement with previous analytical work that considered globular clusters evolving in isolation. The numerical value of the evaporation rate derived with our simulations at R_{GC} = 50 kpc asymptotes to $\xi \approx 0.04$, thus recovering earlier analytical work (Hénon 1961).

5 COMPARISON WITH MOCCA MONTE CARLO MODELS

For comparison, we show in Fig. 5 the time evolution of the mass evaporation rate for two globular clusters once again in different tidal environments, taken from the results of our MOCCA Monte Carlo models. These models are chosen to have identical initial conditions as the *N*-body models shown in Fig. 4 (see Section 2.2). We carefully select MOCCA models that are tidally filling at small R_{GC} and tidally underfilling at large R_{GC}. Two MOCCA models at Galactocentric radii of 50 kpc (black dots) and 4 kpc (blue squares) are shown in Fig. 5.

Fig. 5 shows that the MOCCA simulations are in good agreement with the mass-loss rates ξ seen in the *N*-body models. In particular, MOCCA and *N*-body models agree well on the elevated mass-loss rates due to stellar evolution seen up to about 3 Gyr. Later on, the MOCCA model at $R_{GC} = 4$ kpc evolves faster than the *N*-body model counterpart, that is, this MOCCA model reaches core-collapse faster than the *N*-body model. Post core-collapse, MOCCA models recover earlier analytical predictions for ξ cited in the Introduction and section above. The slightly greater value of ξ for the MOCCA model evolving at $R_{GC} = 4$ kpc can be explained by the stronger tidal field generated by the point mass potential at small galactocentric distances.

We also see increased scatter in the MC results, which is due to the fact that, when calculating ξ at each time-step, the MC method must sample randomly along the stars' orbits to obtain their positions, which induces artificial fluctuations in ξ between time-steps. The *N*-body models avoid this issue altogether by tracking the positions of each star directly at each time-step.

6 EVAPORATION RATE AS A FUNCTION OF TIME AND GALACTOCENTRIC DISTANCE

It can be seen in Figs 1, 3 and 4 that the time evolution of ξ between 3 and 10 Gyr can be approximated by a linear function of the simplest form: $g(t) = a \times t + b$. This linear phase of evolution for ξ follows the rapid decline from large values due to stellar evolution.

We fitted linear functions of the form described above to a series of *N*-body models of globular clusters at different galactocentric distances in order to make a sketch of the evolution of ξ as a function of time and as a function of R_{GC}, thus deriving $\xi(R_{GC}, t)$.

The models we use to derive $\xi(R_{GC}, t)$ are the models presented in Madrid et al. (2012). These are models with an initial number of stars $N = 100\,000$ and initial mass $M_{init} \approx 6.3 \times 10^4\,M_\odot$. We use the models that evolved at 4, 6, 8, 10, 20 and 50 kpc from the Galactic Centre (labels 3–8, Table 1). We have taken the approach of keeping the initial half-mass radius identical for each model. This means the models at small galactocentric distance start tidally filling and become progressively tidally under filling as R_{GC} increases.

We obtain the following expression for $\xi(R_{GC}, t)$

$$\xi(R_{GC}, t) = a \times \log(t) + b \tag{4}$$

where $a(R_{GC})$ and $b(R_{GC})$ are

$$a(R_{GC}) = -10^{(3.0\times\exp(-4.0\times\log(R_{GC}-1.05))-1.2)} \tag{5}$$

and

$$b(R_{GC}) = 10^{(2.5\times\exp(-4.0\times(\log(R_{GC}-0.4))-0.5)} \tag{6}$$

with t in Myr and R_{GC} in kpc, we give the details of its derivation in the appendix.

In Fig. 6, we use equation (4) to sketch the evolution of ξ for a globular cluster that decays into the Galactic Centre. We consider a globular cluster that inspirals into the Galactic Centre through dynamical friction. The dynamical friction time-scale is given by Binney & Tremaine (1987) in their equations 7–26. A globular cluster with an initial mass of $M_{init} \sim 10^5\,M_\odot$ and orbiting at R_{GC} = 15 kpc would take ∼13 000 Gyr to decay into the Galactic Centre by dynamical friction alone. That is, a thousand times a Hubble time. The mass evaporation rate and the distance to the centre of the galaxy are depicted on the top panel of Fig. 6. ξ undergoes a marked increase as the globular cluster approaches the centre of the galaxy (see below). We do not directly address the magnitude of the dynamical friction time-scale, as this has been looked at in detail in previous studies, e.g. Gnedin et al. (2014).

For a globular cluster that inspirals to the Galactic Centre, the dimensionless mass evaporation rate, as given by equation (4), increases by a factor of 32 during the time the orbit of the globular cluster decays from $R_{GC} = 14$ kpc to $R_{GC} = 4$ kpc. The trend is clear towards the centre of the galaxy where our results suggest that ξ continues to increase within the inner 4 kpc. As ξ is extrapolated inwards, it re-approaches the very high values seen very early on due to stellar evolution. We should note that the factor of 32

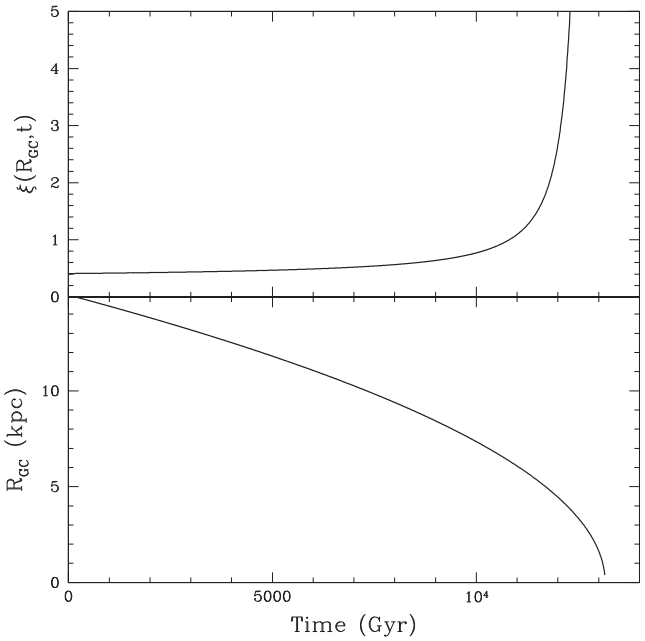

Figure 6. Evolution of $\xi(R_{gc}, t)$ for a globular cluster that decays into the Galactic Centre. The top panel depicts the evolution of ξ for a globular cluster that inspirals into the Galactic Centre following the dynamical friction time-scale given by Binney and Tremaine (1987). We find a marked increase of the value of ξ as the globular cluster approaches the centre of the galaxy. Note that top and bottom quantities scale as the inverse of the other and this is highlighted by the log y-scale of the bottom panel.

increase is also dependent on the initial conditions of the star cluster, for instance, its initial half-mass radius.

The extrapolation of our results to lower galactocentric distances illustrates that the value of ξ could reach or even exceed the previous maximum value of ∼6.9 due to stellar evolution. This result serves to highlight the importance of developing a better understanding on how a globular cluster responds to extreme tidal striping by the galactic potential in the inner regions of a galaxy. A more detailed analysis of the behaviour of ξ towards the core of the galaxy, including a more detailed modelling of the bulge potential, will be presented by Rossi et al. (in preparation).

Our results support the conclusions reached by Webb & Leigh (2015), namely that modern simulations of GC evolution are still underestimating the mass-loss. The authors presented a method for estimating the total initial masses in Galactic globular clusters, using only the total cluster luminosity or mass and the slope of the present-day stellar mass function. The results of Webb & Leigh (2015) are in good agreement with earlier findings of Vesperini & Heggie (1997) and Kruijssen (2009).

An evaporation rate that clearly rises as the globular cluster approaches the Galactic Centre should certainly be accounted for in future models that propose to explain the formation of nuclear star clusters by infalling globular clusters, e.g. Gnedin et al. (2014).

In terms of the overall mass-loss rates, using the recent results of Webb & Leigh (2015) and Cai et al. (2016), we expect that the time-averaged mass-loss rate for any given eccentricity can be approximately set equal to the rate for a circular orbit at a given Galactocentric distance, which is slightly larger than pericentre, typically, but obviously smaller than apocentre for the eccentric orbit. It is not known, however, how an eccentric orbit affects the dynamical friction time-scale itself. Functions like the ones provided for $\xi(R_{GC}, t)$ can be used to properly calculate the fate of a GC that loses mass as it spirals into the nucleus due to dynamical friction.

7 FORMATION OF NUCLEAR STAR CLUSTERS BY INSPIRALLING GLOBULAR CLUSTERS

Globular clusters are affected by dynamical friction that makes them inspiral into the centre of their host galaxy, possibly providing material to create nuclear star clusters (Tremaine, Ostriker & Spitzer 1975; Leigh, Böker & Knigge 2012b; Antonini 2013; Arca-Sedda & Capuzzo-Dolcetta 2014; Gnedin et al. 2014).

A caveat to the above theory is the dissolution of infalling globular clusters before reaching the nuclear region. Dynamical friction is a function of mass. While a globular cluster as an entire entity can experience enough dynamical friction to infall into the Galactic Centre, its individual stars, once lost due to tidal heating, are practically unaffected by dynamical friction (Tremaine et al. 1975).

Dynamical friction time-scales dictate that only massive globular clusters that orbit a galaxy within a few (∼3–6 kpc) would spiral to the Galactic Centre during a Hubble time, see the example for the Andromeda galaxy by Binney & Tremaine (1987). We have shown here that it is precisely in this region that the evaporation rate of globular clusters is higher than previously thought. This implies a smaller mass budget to build nuclear star clusters from infalling globular clusters. Our models show that any globular cluster spiralling into the nucleus will lose a significant fraction of its total initial mass, with that fraction being close to unity (Webb & Leigh 2015).

Arca-Sedda & Capuzzo-Dolcetta (2014) recently modelled the origin of nuclear star clusters from migratory globular clusters. They found that when the effects of tidal shocks were included in their models, the number of globular clusters that effectively spiral into the nucleus of the galaxy decreased by a factor of 5. Arca-Sedda & Capuzzo-Dolcetta (2014) even found that for their models of massive galaxies with tidal heating, the number of globular clusters falling into the Galactic Centre drops to zero, preventing the formation of a nuclear star cluster.

Through this work, we have shown that when stellar evolution and the galactic tidal field are included into the models of globular clusters, their dimensionless mass evaporation rate is much higher than previously presented. We have also derived the dependence of ξ on galactocentric distance and time, quantifying how the evaporation rate of globular clusters is enhanced as they approach the Galactic Centre.

We would like to highlight the importance of properly understanding mass-loss in the inner Galactic potential, which is still highly uncertain. In particular, our results show that mass-loss in the inner Galaxy could be significant. Even accounting for *all* sources of mass-loss in our estimate for ξ, our theoretical extrapolation suggests, it could rise above even the ξ values we see at early times when stellar evolution dominates (included in our $\xi(M)$ estimate). Although our simple theoretical extrapolation of the mass-loss rate to the inner Galactic potential diverges at $r = 0$ (see Fig. 5), the true mass-loss rate should not become infinite. Whether or not the true mass-loss rate does indeed get this high is an open question and could significantly affect previous estimates of the mass-loss rates used for calculations involving nuclear star cluster formation via globular cluster inspiral.

ACKNOWLEDGEMENTS

We would like to thank the anonymous referees for providing detailed reports that helped us improve this paper. This research has made use of the NASA Astrophysics Data System Bibliographic services (ADS) and Google. This work was performed on the gSTAR national facility at Swinburne University of Technology. gSTAR is funded by Swinburne and the Australian Government Education Investment Fund. This research was supported by Australian Research Council funding through grant DP110103509. MG acknowledges support from the National Science Centre through the grant DEC-2012/07/B/ST9/04412.

REFERENCES

Aarseth S. J., 1999, PASP, 111, 1333
Aarseth S. J., 2003, Gravitational N-body Simulations: Tools and Algorithms (Cambridge Monographs on Mathematical Physics). Cambridge Univ. Press, Cambridge
Ambartsumian V. A., 1938, Uch. Zap. LGU, 22, 19 (English translation in Goodman J., Hut P., eds, Proc. IAU Symp. 113, Dynamics of Star Clusters. Reidel, Dordrecht, p. 521)
Antonini F., 2013, ApJ, 763, 62
Arca-Sedda M., Capuzzo-Dolcetta R., 2014, MNRAS, 444, 3738
Baumgardt H., 2001, 325, 1323
Baumgardt H., Makino J., 2003, MNRAS, 340, 227
Binney J., Tremaine S., 1987, Galactic Dynamics. Princeton Univ. Press, Princeton, NJ, p. 514
Brockamp M., Küpper A. H. W., Thies I., Baumgardt H., Kroupa P., 2014, MNRAS, 441, 150
Cai M. X., Gieles M., Heggie D. C., Varri A. L., 2016, MNRAS, 455, 596
Fukushige T., Heggie D. C., 2000, MNRAS, 318, 753
Gieles M., Baumgardt H., 2008, MNRAS, 389, L28
Gieles M., Heggie D. C., Zhao H., 2011, MNRAS, 413, 2509
Giersz M., Heggie D. C., 1996, MNRAS, 279, 1037
Giersz M., Heggie D. C., Hurley J. R., Hypki A., 2013, MNRAS, 431, 2184
Gnedin O. Y., Ostriker J. P., 1997, ApJ, 474, 223
Gnedin O. Y., Ostriker J. P., Tremaine S., 2014, ApJ, 785, 71
Heggie D. C., 2011, Bull. Astron. Soc. India, 39, 69
Heggie D. C., 2014, MNRAS, 445, 3435
Hénon M., 1961, Ann. Astrophys., 24, 369
Hong J., Kim E., Lee H. M., Spurzem R., 2013, MNRAS, 430, 2960
Hurley J. R., Pols O. R., Tout C. A., 2000, MNRAS, 315, 543
Hurley J. R., Tout C. A., Pols O. R., 2002, MNRAS, 329, 897
Hypki A., Giersz M., 2013, MNRAS, 429, 1221
Kroupa P., 2001, MNRAS, 322, 231
Kruijssen J. M. D., 2009, A&A, 507, 1409
Kruijssen J. M. D., 2015, MNRAS, 454, 1658
Kruijssen J. M. D. et al., 2012, MNRAS, 421, 1927
Küpper A. H., Kroupa P., Baumgardt H., Heggie D. C., 2010, MNRAS, 401, 105
Lamers H. J. G. L. M., Baumgardt H., Gieles M., 2010, MNRAS, 409, 305
Lee H. M., Goodman J., 1995, ApJ, 443, 109
Leigh N. W. C., Umbreit S., Sills A., Perets H. B., Sarajedini A., Glebbeek E., 2012a, MNRAS, 422, 1592
Leigh N., Böker T., Knigge C., 2012b, MNRAS, 424, 2130
Leigh N. W. C., Giersz M., Webb J. J., Hypki A., De Marchi G., Kroupa P., Sills A., 2013, MNRAS, 436, 339
Madrid J. P., Hurley J. R., Sippel A. C., 2012, ApJ, 756, 167
Madrid J. P., Hurley J. R., Martig M., 2014, ApJ, 784, 95
Miyamoto M., Nagai R., 1975, PASJ, 27, 533
Planck Collaboration XIII, 2016, A&A, 594, 13
Plummer H. C., 1911, MNRAS, 71, 460
Pols O., Schröder K-P., Hurley J. R., Tout C. A., Eggleton P. P., 1998, MNRAS, 298, 525
Spitzer L., 1940, MNRAS, 100, 397
Spitzer L., Chevalier R. A., 1973, ApJ, 183, 565
Spitzer L., Hart M. H., 1971, ApJ, 164, 399
Takahashi K., Portegies Zwart S. F., 2000, ApJ, 535, 759
Tremaine S. D., Ostriker J. P., Spitzer L., 1975, ApJ, 196, 407
Vesperini E., Heggie D. C., 1997, MNRAS, 289, 898
von Hoerner S., 1957, ApJ, 125, 451
Wang L. et al., 2016, MNRAS, 458, 1450
Webb J. J., Leigh N. W. C., 2015, MNRAS, 453, 3278
Webb J. J., Sills A., Harris W. E., 2013, ApJ, 779, 94
Webb J. J., Leigh N. W. C., Sills A., Harris W. E., Hurley J. R., 2014, MNRAS, 442, 1569

APPENDIX: DERIVATION OF $\xi(R_{\rm GC}, t)$

This appendix presents the details of the derivation of $\xi(R_{\rm GC}, t)$. In order to derive $\xi(R_{\rm GC}, t)$, we assume that ξ varies smoothly as a function of $R_{\rm GC}$ and that it takes the following general functional form:

$$\xi(R_{\rm GC}, t) = f(R_{\rm GC}) \times g(t) \tag{A1}$$

for some unknown functions f and g.

We also assume that the temporal component takes the following form $g(t) = a \times \log(t) + b$. As mentioned in Section 5, the linear part of the temporal evolution of ξ for the numerical models is between 3 and 10 Gyr. Replacing $g(t)$ into the general expression for ξ, we obtain:

$$\xi(R_{\rm GC}, t) = f(R_{\rm GC}) \times (a \times \log(t) + b) \tag{A2}$$

or

$$\xi(R_{\rm GC}, t) = f(R_{\rm GC}) \times a \times \log(t) + f(R_{\rm GC}) \times b, \tag{A3}$$

By absorbing the constants a and b into the functions f and g, respectively, $\xi(R_{\rm GC}, t)$ can be re-written as

$$\xi(R_{\rm GC}, t) = a(R_{\rm GC}) \times \log(t) + b(R_{\rm GC}). \tag{A4}$$

We fit straight lines to the value of $\xi(t)$ derived with the simulations between ∼3 and 10 Gyr.

We then take the slopes (i.e. a) and y intercepts (i.e. b) of the fitted lines (in blue in Fig. A1 of the appendix). The slopes and intercepts define six points (one for each galactocentric distance) in the $\log(R_{\rm GC}) - \log(a)$ and $\log(R_{\rm GC}) - \log(b)$ space, as shown in Fig. A2. Using least-squares linear regression, these points are described by the following expressions:

$$a(R_{\rm GC}) = -10^{(3.0\times\exp(-4.0\times\log(R_{\rm GC}-1.05))-1.2)} \tag{A5}$$

and

$$b(R_{\rm GC}) = 10^{(2.5\times\exp(-4.0\times(\log(R_{\rm GC}-0.4))-0.5)}. \tag{A6}$$

We thus can finally write $\xi(R_{\rm GC}, t)$ as

$$\xi(R_{\rm GC}, t) = a \times \log(t) + b \tag{A7}$$

with t in Myr and $R_{\rm GC}$ in kpc.

As mentioned above, this expression of $\xi(R_{\rm GC}, t)$ is valid between ∼3 and 10 Gyr. For a representation of $\xi(R_{\rm GC}, t)$ between 0 and 3 Gyr, we suggest a linear interpolation between an initial global value of 6.9 to the value given by equation (3) at 3 Gyr for the orbit of choice. A minimum of 0.05 can be applied to equation (3) to make it valid at later times.

The equations derived for $\xi(R_{\rm GC}, t)$ are meant as an example of the proposed method for calculating $\xi(t)$ from a series of cluster simulations for a given set of initial conditions. It is valid for a given initial half-mass radius $r_{{\rm hm},i}$ (and concentration) and initial total cluster mass M_i. We fix these two quantities in deriving our

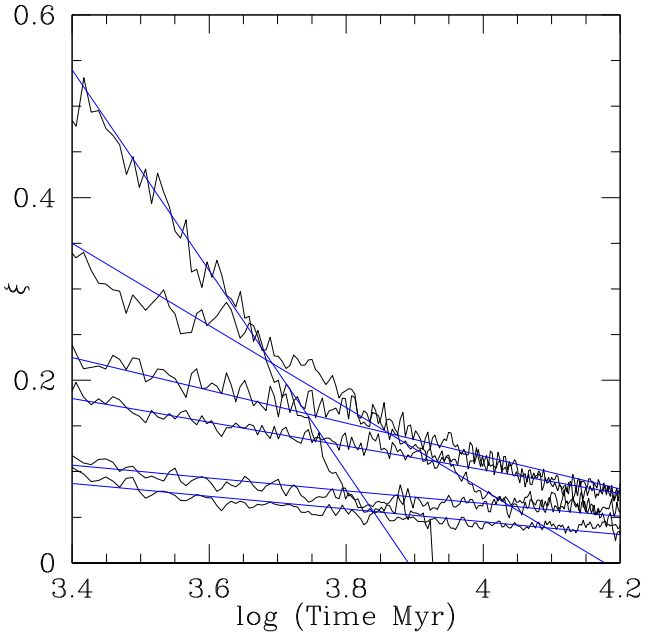

Figure A1. Fits to the values of ξ for the following galactocentric distances, from top to bottom: 4, 6, 8, 10, 20, 50 kpc.

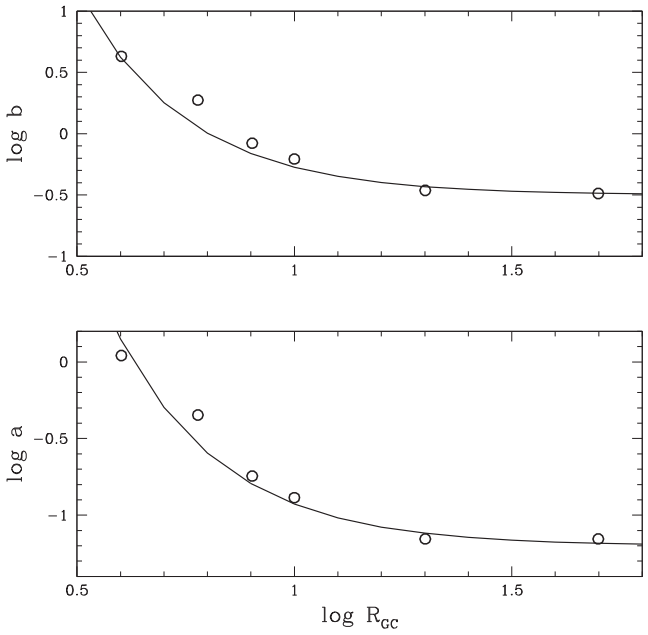

Figure A2. Slopes (i.e. a) and y intercepts (i.e. b) of the fitted lines (in blue in Fig. A1 of the appendix). The solid lines show least-squares fits to the data in ln–ln-space.

equations in this appendix, which results in different initial degrees of tidal filling as a function of galactocentric distance. This is meant to provide a reasonable, albeit approximate, method of calculating a solution to the dynamic mass-loss rate (which changes over time due to various effects, such as stellar evolution) as $R_{\rm GC}$ decreases due to dynamical friction by iterating between the equations for $\xi(R_{\rm GC}, t)$ provided by our N-body simulations evolved at different $R_{\rm GC}$. Hence, our solution for $\xi(t)$ for a globular cluster with a given set of initial $r_{h,i}$ and M_i values should appear as a line tilted in the time-ξ plane in the figure shown in this appendix. The slope of this line should change if the rate of decrease of galactocentric distance due to dynamical friction changes.

In future work, we intend to populate a grid of $\xi(R_{\rm GC}, t)$ solutions by obtaining the parameters a and b in our fitting functions for different $r_{\rm hm,i}$ and M_i values in additional N-body simulations. That is, we will apply the same method as described in this paper to analogous sets of N-body models with different $r_{h,i}$ and M_i values. This will populate the parameter space for $\xi(t)$ relevant to the Milky Way globular cluster population. Our method folds into a single ξ parameter all of the relevant physics (e.g. stellar evolution mass-loss, relaxation-driven mass-loss, etc.), such that a single analytic function describes the complex interplay between these physical processes.

Populating a grid in $r_{\rm hm,i}$ and M_i with simulated clusters would be prohibitively expensive using N-body simulations but entirely feasible using the Monte Carlo method for globular cluster evolution. Our comparison to the MOCCA simulations could then be used to interpret the results of the experiment described above.

This paper has been typeset from a TEX/LATEX file prepared by the author.